Structural Studies of Oriented Zirconium Bis(phosphonoacetic acid) Using Solid-State ^{31}P and ^{13}C NMR

David A. Burwell, Kathleen G. Valentine, Jozef H. Timmermans, and Mark E. Thompson*

Contribution from the Department of Chemistry, Princeton University, Princeton, New Jersey 08544. *Received August 26, 1991*

Abstract: Solid-state ^{31}P and ^{13}C NMR spectra of uniaxially oriented films of layered zirconium bis(phosphonoacetic acid) are discussed. Prior determination of the ^{31}P phosphonate and ^{13}C carboxyl chemical shielding tensors in $Zr(O_3PCH_2COOH)_2$ allowed for quantitative interpretation of the chemical shift frequencies exhibited in these spectra. Structural details of the organic pendant group are elucidated by analyzing the oriented chemical shift frequency in terms of its dependence on the orientation of the chemical shielding principal axes in the static magnetic field. In $Zr(O_3PCH_2COOH)_2$, the P–C bond was determined to lie perpendicular to the inorganic layers, and the P–C–C–O dihedral angle was calculated as 90 ± 15°.

Introduction

Intercalation reactions of layered zirconium phosphonates have been a recent focus of several groups' attention as a means for preparing new materials with tailored solid-state structures and properties. Of particular interest to us is the intercalation chemistry of a family of carboxy-terminated zirconium phosphonates, $Zr(O_3P(CH_2)_nCOOH)_2$.[1-5] These compounds can be precipitated as microcrystalline solids and, for n = 1–5, have interlayer spacings ranging from approximately 11 to 19 Å, respectively.[6] We have found that changing the number of methylene spacers, n, between the inorganic zirconium phosphate-type layers (i.e., $Zr(O_3P-)_2$) and the carboxy group affects the latter's reactivity toward both organic and inorganic guest molecules.[5] It is likely that this variation in reactivity is related to solid-state packing-induced structural changes in the pendant organic group that alter the hosts' ability to interact with guest molecules. Structural changes resulting from both interlayer dimer-type hydrogen bonding of the carboxylic acid groups and an odd/even n effect (Figure 1) are expected to be important. A detailed investigation of the proton conductivity of these same carboxy-terminated zirconium phosphonates was very recently reported by Alberti et al.[7] Their results showed that the n = 1, 3, and 5 compounds exhibit much higher conductivity than the n = 2 and 4 compounds. They too propose that structural changes associated with an odd/even n effect are responsible for this behavior. We would like to better understand these changes and any effect they might have on the chemical and physical properties of $Zr(O_3P(CH_2)_nCOOH)_2$. Unfortunately, zirconium phosphonate crystals of sufficient size for structural determination by conventional X-ray diffraction (XRD) techniques have yet to be grown. In lieu of XRD analysis, we have initiated a solid-state multinuclear NMR study aimed at resolving the structures of the organic moiety in $Zr(O_3P(CH_2)_nCOOH)_2$.

In previous work, we determined the ^{31}P phosphonate and ^{13}C carboxyl chemical shielding tensors in $Zr(O_3PCH_2COOH)_2$ by matching simulated and experimental dipolar coupled powder patterns of selectively ^{13}C labeled compounds.[8] Both the orientations of the chemical shielding tensors in the molecular frame and the distances between the nuclei of the P–C–C fragment were established (Figure 2). In the present work, we use this chemical shielding tensor information to analyze the chemical shifts observed in solid-state ^{31}P and ^{13}C NMR spectra of uniaxially oriented films of $Zr(O_3PCH_2{}^{13}COOH)_2$. Our goal is to elucidate structural details of the organic fragment (such as the P–C bond and COOH plane orientations relative to the $Zr(O_3P-)_2$ layers) by combining the angular information inherent in the chemical shift anisotropy (CSA) with knowledge of the chemical shielding tensor orientation in the molecular frame.

The experimental method employed here is a variation of that used by Cornell et al.[9] and Nicholson and Cross[10] to determine the secondary structure of gramicidin A incorporated into dimyristoylphosphatidylcholine (DMPC) bilayers by solid-state ^{13}C and ^{15}N NMR spectroscopies, respectively. It consists of three steps. First, the sample is prepared in a manner such that at least one of its crystallographic axes can be oriented relative to the static magnetic field vector, $\mathbf{B}_0$. In the work on gramicidin A, formation of DMPC bilayer membranes on glass slides allowed the bilayer director to be used as the axis of orientation. Here, the observation that the sheet-like microcrystallites of zirconium phosphonate (Figure 3C) uniformly orient on planar surfaces allowed us to use the $Zr(O_3P-)_2$ layer normal as the axis of orientation. Uniaxial sample orientation was attained by casting a sonicated ethanol dispersion of $Zr(O_3PCH_2{}^{13}COOH)_2$ onto 6 × 22 mm pieces of microscope slide cover glass. Upon evaporation, the dispersion leaves a thin film that consists of microcrystalline $Zr(O_3PCH_2{}^{13}COOH)_2$ platelets lying parallel to the cover glass (Figure 3B). (It may be useful to envision the orientation of the sample platelets on the cover glass as a deck of cards tossed on the floor.) Optical microscopy shows that the majority of the thin film is well aligned and 1 to 3 crystals thick. Much thicker (>20 crystals), poorly aligned regions are also present, mostly on the edges of the film. Twenty-five cover glass slides were stacked in a sample cylinder, which was then placed in the NMR probe coil with the $Zr(O_3P-)_2$ layer normal parallel to $\mathbf{B}_0$ (Figure 3A). The orientation of layer normal relative to $\mathbf{B}_0$ was controlled by rotating the stack of film coated slides in the probe coil.

In the second step, the chemical shift frequencies observed in spectra of the oriented sample are analyzed to determine possible orientations of the chemical shielding principal axis system (PAS) relative to $\mathbf{B}_0$. The chemical shielding PAS is an orthogonal coordinate system that describes the three-dimensional magnetic shielding of a nucleus by surrounding electrons.[11] Quantitative

* Author to whom correspondence should be addressed.

(1) (a) Alberti, G.; Costantino, U.; Giovagnotti, M. L. L. *J. Chromatogr.* **1979**, *180*, 45. (b) Alberti, G.; Costantino, U. In *Intercalation Chemistry*; Whittingham, M. S., Jacobson, A. J., Eds.; Academic Press Inc.: New York, 1982; Chapter 5. (c) Alberti, G.; Costantino, U. *J. Mol. Catal.* **1984**, *27*, 235.

(2) (a) Környei, J.; Szirtes, L. *J. Radio. Nucl. Chem.* **1984**, *83* (2), 257. (b) Környei, J.; Szirtes, L.; Costantino, U. *J. Radio. Nucl. Chem.* **1985**, *89* (2), 331.

(3) (a) Clearfield, A. In *Design of New Materials*; Cocke, D. L., Clearfield, A., Eds.; Plenum Press: New York, 1988; p 121. (b) Clearfield, A. *Comments Inorg. Chem.* **1990**, *10*, 89.

(4) Cao, G.; Rabenberg, L. K.; Nunn, C. M.; Mallouk, T. E. *Chem. Mater.* **1991**, *3*, 149.

(5) (a) Burwell, D. A.; Thompson, M. E. *Chem. Mater.* **1991**, *3*, 14. (b) Burwell, D. A.; Thompson, M. E. *Chem. Mater.* **1991**, *3*, 730.

(6) Dines, M. B.; DiGiacomo, P. M. *Inorg. Chem.* **1981**, *20*, 92.

(7) Alberti, G.; Costantino, U.; Casciola, M.; Vivani, R.; Peraio, A. *Solid State Ionics* **1991**, *46*, 61.

(8) Burwell, D. A.; Valentine, K. G.; Thompson, M. E. *J. Magn. Reson.*, in press.

(9) Cornell, B. A.; Separovic, F.; Baldassi, A. J.; Smith, R. *Biophys. J.* **1988**, *53*, 67.

(10) Nicholson, L. K.; Cross, T. A. *Biochemistry* **1989**, *28*, 9379.

0002-7863/92/1514-4144$03.00/0 © 1992 American Chemical Society

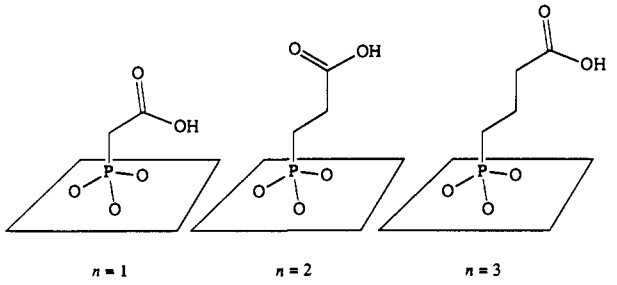

Figure 1. Idealized representation of the effect of odd vs even n on the carboxy plane orientation in $Zr(O_3P(CH_2)_nCOOH)_2$.

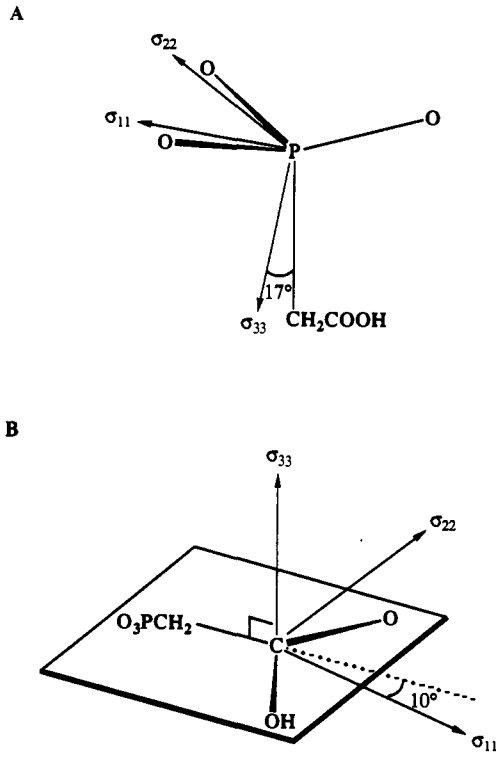

Figure 2. Orientation of the (A) ^{31}P and (B) ^{13}C chemical shielding tensors in the molecular frame of $Zr(O_3PCH_2COOH)_2$.

structural analysis via the oriented spectra requires calculations based on the mathematical expression relating the observed oriented chemical shift frequency to the geometric disposition of $\mathbf{B}_0$ in the chemical shielding PAS. Once the orientation of the chemical shielding PAS relative to $\mathbf{B}_0$ is known, the $Zr(O_3P-)_2$ layer normal may be geometrically transformed to the PAS through the $\mathbf{B}_0$ reference frame.

In the final step, the $Zr(O_3P-)_2$ layer normal is related to the molecular frame by a second geometric transformation of the layer normal through the chemical shielding PAS. This last step depends on the prior determination of the chemical shielding PAS orientation relative to the molecular frame in $Zr(O_3PCH_2COOH)$.

There are a few accounts in the literature of solid-state NMR studies that use the chemical shift's orientational dependence to determine structures of uniaxially oriented samples. For example, Griffin et al. determined the orientation of the phospholipid head group in oriented dipalmitoylphosphatidylcholine (DPPC) bilayers by analyzing ^{31}P phosphate oriented chemical shift frequencies.[12] More recently, Opella, Cross, and co-workers analyzed ^{15}N amide and ^{13}C carbonyl oriented chemical shift frequencies to elucidate peptide plane orientations in proteins.[13] Liquid crystalline polymers have also been the focus of oriented sample CSA studies.[14,15] Spiess et al. recently reported the application of a solid-state ^{13}C NMR technique very similar to the one employed here to the study of oriented liquid crystalline polymer thin films.[14] They correlated alignment perturbations of a liquid crystalline matrix with the optical isomerization of a cyanoazobenzene dye incorporated in the polymer. To assay these perturbations, the ^{13}C chemical shifts of the dye's ^{13}C-labeled cyano group were analyzed as the orientation of the director of the liquid crystalline thin film was varied relative to $\mathbf{B}_0$.

In work on systems more closely resembling ours, Resing and co-workers used solid-state NMR spectroscopy to study the orientation and dynamics of guest molecules intercalated in highly oriented pyrolytic graphite (HOPG) and in an oriented clay.[16] Particularly relevant work involved the analysis of ^{13}C chemical shifts obtained from oriented samples of sedimented hectorite clay intercalated with benzene.[16a]

As interest in using layered metal phosphonates in materials and catalysis research grows, the need for tools to characterize their solid-state structures increases as well. Described herein is a solid-state NMR experiment useful for determining structures of organic pendant groups in these compounds. Although the conceptual basis for the experiment is not new, this is the first report of the application of such an experiment to layered metal phosphonates. And, while the present work focuses on the analysis of ^{31}P phosphonate and ^{13}C carboxyl chemical shifts, this technique may be readily applied to other functional groups containing NMR-active nuclei that exhibit significant chemical shift anisotropies.

Theory

The resonance frequency of a nucleus in the solid state depends to a first approximation on chemical shielding and dipolar perturbations of the nuclear Larmor precession frequency. The anisotropic chemical shielding of the nucleus can be expressed as a second rank tensor, σ. Diagonalization of σ yields the three principal tensor elements, σ_{11}, σ_{22} and σ_{33}, that together constitute the principal axes of the orthogonal coordinate system referred to as the chemical shielding PAS. The observed chemical shift of the nucleus depends on the orientation of the chemical shielding PAS relative to $\mathbf{B}_0$. That orientation can be described by two Euler angles, ϕ and θ. As depicted in Figure 4, θ is defined as the angle between $\mathbf{B}_0$ and the principal element σ_{33}, while ϕ is defined as the angle between σ_{11} and the projection of $\mathbf{B}_0$ in the σ_{11}–σ_{22} plane.

In a random microcrystalline powder, all orientations of the chemical shielding PAS relative to $\mathbf{B}_0$ exist, and the resulting NMR spectrum exhibits a broad range of resonance frequencies, i.e., a powder pattern. For a single crystal, where only one orientation exists for each crystallographically unique nucleus, a single resonance is observed within the frequency range of the powder pattern. The spectrum of a uniaxially oriented microcrystalline powder may resemble that of a single crystal, a powder, or something in between, depending on the disposition of the axis of orientation (here, the $Zr(O_3P-)_2$ layer normal) relative to $\mathbf{B}_0$. For example, when the layer normal is coincident with $\mathbf{B}_0$, θ and ϕ will be constant from platelet to platelet within the sample, leading to a single resonance frequency, just as in the case of a single crystal. However, when the layer normal is perpendicular

(11) See, for example: Fyfe, C. A. *Solid-State NMR for Chemists*; C. F. C. Press: Ontario, Canada, 1982; Chapter 5.

(12) Griffin, R. G.; Powers, L.; Pershan, P. S. *Biochemistry* **1978**, *17*, 2718.

(13) (a) Cross, T. A.; Opella, S. J. *J. Am. Chem. Soc.* **1983**, *105*, 306. (b) Cross, T. A.; Opella, S. J. *J. Mol. Biol.* **1985**, *182*, 367. (c) Cross, T. A. *Biophys. J.* **1986**, *49*, 124. (d) Opella, S. J.; Stewart, P. L.; Valentine, K. G. *Q. Rev. Biophys.* **1987**, *19*, 7.

(14) Wiesner, U.; Schmidt-Rohr, K.; Boeffel, C.; Pawelzik, U.; Spiess, H. W. *Adv. Mater.* **1990**, *2*, 484.

(15) Oulyadi, H.; Lauprêtre, F.; Monnerie, L.; Mauzac, M.; Richard, H.; Gasparoux, H. *Macromolecules* **1990**, *23*, 1965.

(16) (a) Resing, H. A.; Slotfelt-Ellingsen, D.; Garroway, A. N.; Pinnavaia, T. J.; Unger, K. In *Magnetic Resonance in Colloid and Interface Science*; Fraissard, J. P., Resing, H. A., Eds.; D. Reidel Publishing Company: Dordecht, Holland, 1979. (b) Resing, H. A.; Slotfeldt-Ellingsen, D. *J. Magn. Reson.* **1980**, *38*, 401. (c) Miller, G. R.; Resing, H. A.; Moran, M. J.; Banks, L.; Vogel, F. L.; Pron, A.; Billaud, D. *Synth. Met.* **1983**, *8*, 77. (d) Miller, G. R.; Poranski, C. F.; Resing, H. A. *J. Chem. Phys.* **1984**, *80* (4), 1708. (e) Miller, G. R.; Moran, M. J.; Resing, H. A.; Tsang, T. *Langmuir* **1986**, *2*, 194.

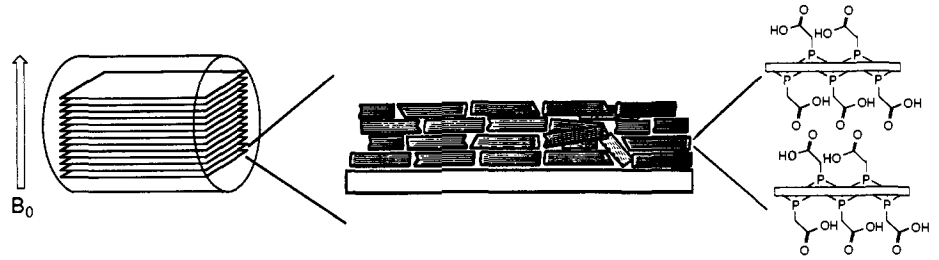

Figure 3. Schematic representations of (A, left) a layer normal oriented parallel to $\mathbf{B}_0$ in the NMR sample cylinder, (B, middle) $Zr(O_3PCH_2COOH)_2$ crystallites on a glass slide, and (C, right) a 2-D layered structure of $Zr(O_3PCH_2COOH)_2$.

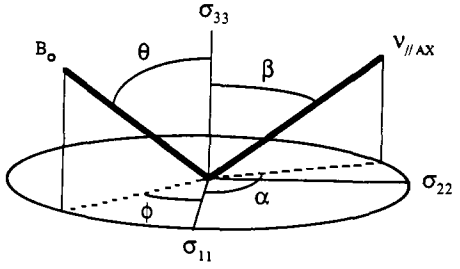

Figure 4. Description of the magnetic field vector, $\mathbf{B}_0$, and the unique element of the dipolar interaction tensor, $\nu_{//AX}$, in the chemical shielding principal axis system (PAS).

to $\mathbf{B}_0$, a range of θ and ϕ values results, leading to a broad line shape (vide infra).

When the nucleus is part of an isolated spin pair, AX, the observed resonance frequency will also depend on the orientation of the unique element of the direct dipolar tensor (i.e., $\nu_{//AX}$, or the A–X internuclear vector) relative to the chemical shielding PAS. This orientation can be defined by the Euler angles, α and β, shown in Figure 4. The NMR spectrum of a single crystal or an oriented microcrystalline powder will exhibit a doublet of splitting $D\{1 - 3[\sin\beta \sin\theta \cos(\phi - \alpha) + \cos\beta \cos\theta]^2\}$, where D is the dipolar coupling constant. In addition to the relatively large chemical shielding and dipolar perturbations, indirect spin–spin coupling, or J-coupling, will further perturb the resonance frequency, but to a lesser extent. For $Zr(O_3PCH_2{}^{13}COOH)_2$, 2-bond through-space ^{31}P–$^{13}C(O)$ dipolar coupling is important but J-coupling between these nuclei is insignificant.[8] Thus, the observed resonance frequency for the ^{31}P nuclei in a uniaxially oriented sample of $Zr(O_3PCH_2{}^{13}COOH)_2$ can be expressed by the following equations:

$$\nu_P(\theta,\phi) = \nu_L - \nu_{CS} - m_C\nu_D \quad (1)$$

$$\nu_L = \gamma_P\mathbf{B}_0/2\pi \quad (2)$$

$$\nu_{CS}(\theta,\phi) = \sigma_{11}\cos^2\phi\sin^2\theta + \sigma_{22}\sin^2\phi\sin^2\theta + \sigma_{33}\cos^2\theta \quad (3)$$

$$\nu_D(\theta,\phi,\alpha,\beta) = D_{PC}\{1 - 3[\sin\beta\sin\theta\cos(\phi - \alpha) + \cos\beta\cos\theta]^2\} \quad (4)$$

$$D_{PC} = (\mu_0/4\pi)\gamma_P\gamma_C(h/4\pi^2)r_{PC}^{-3} \quad (5)$$

where ν_P is the resonance frequency for the P nuclei, ν_L is the Larmor precession frequency of the "bare" phosphorus nucleus, ν_{CS} is the chemical shielding frequency, m_C is the spin quantum number of the carbon nucleus (i.e., $\pm^1/_2$), ν_D is the ^{31}P–^{13}C dipolar coupling interaction frequency, σ_{ii} are the principal elements of the ^{31}P chemical shielding tensor, and D_{PC} is the maximum ^{31}P–^{13}C dipolar coupling constant. Analogous expressions can be derived for the resonance frequency of the ^{13}C nuclei.

Results and Discussion

Phosphorus-31 NMR Spectra of $Zr(O_3PCH_2{}^{13}COOH)$. Oriented ^{31}P cross-polarized (CP) NMR spectra of ^{13}C-labeled $Zr(O_3PCH_2{}^{13}COOH)_2$ are presented in Figure 5. On the left side of Figure 5 are shown the experimental CSA powder pattern (C), the experimental spectrum with the layer normal perpendicular to $\mathbf{B}_0$ (B), and the difference spectrum (A). The analogous spectra obtained with the layer normal parallel to $\mathbf{B}_0$ are shown on the right side of Figure 5. The effect of uniaxial sample orientation is readily seen by comparing the two difference spectra.[17] The resonance frequencies seen in the perpendicular difference spectrum fall exclusively in the σ_{11}–σ_{22} region of the CSA powder pattern, whereas frequencies in the σ_{33} region were observed in the parallel difference spectrum. These spectra indicate, in a qualitative sense, that σ_{33} was nearly coincident with $\mathbf{B}_0$ when the $Zr(O_3P–)_2$ layer normal was parallel to $\mathbf{B}_0$ and that σ_{33} was nearly perpendicular to $\mathbf{B}_0$ when the layer normal was perpendicular to $\mathbf{B}_0$.

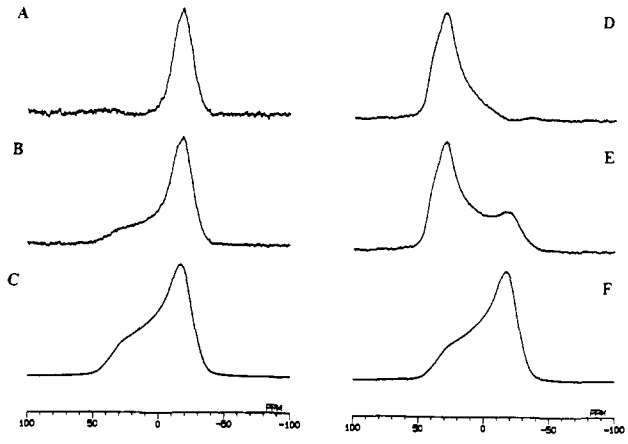

Figure 5. 109.4-MHz ^{31}P CP NMR spectra of oriented $Zr(O_3PCH_2{}^{13}COOH)_2$: (A) perpendicular difference spectrum, (B) perpendicular experimental spectrum, (C) experimental powder spectrum, (D) parallel difference spectrum, (E) parallel experimental spectrum, and (F) experimental powder spectrum.

The oriented spectra were quantitatively interpreted using eq 3—which relates the observed chemical shift to the orientation of $\mathbf{B}_0$ in the chemical shielding PAS—and the predetermined orientation of the ^{31}P phosphonate chemical shielding PAS in the molecular frame of $Zr(O_3PCH_2COOH)_2$.[8] When the layer normal was positioned parallel to $\mathbf{B}_0$, the resulting difference spectrum (Figure 5D) exhibited an asymmetric band of resonance frequencies centered at 30 ppm. To simplify analysis of the line shape, the observed range of chemical shifts was taken as the full width at half maximum intensity. Thus, the range of chemical shift in the parallel difference spectrum is 30 ± 10 ppm. The chemical shielding tensor principal elements extracted from the CSA powder pattern were the following: σ_{11} = +26 ppm, σ_{22} = +14 ppm, and σ_{33} = −40 ppm. θ/ϕ combinations resulting in chemical shifts within the 30 ± 10 ppm range were then calculated using eq 3 and the principal elements. The θ/ϕ combinations consistent with the chemical shifts exhibited in the parallel difference spectrum are represented by the shaded region in Figure 6B. On the basis of this plot, θ was limited to 0–34°. Note that

(17) As mentioned, some disorder (i.e., platelet non-alignment) was observed at the edges of the cover slips, leading to powder-type (i.e., amorphous) contributions to the observed line shapes in the oriented spectra. To remove these powder-type contributions, it was necessary to subtract approximately 40% powder pattern from each oriented experimental spectrum.

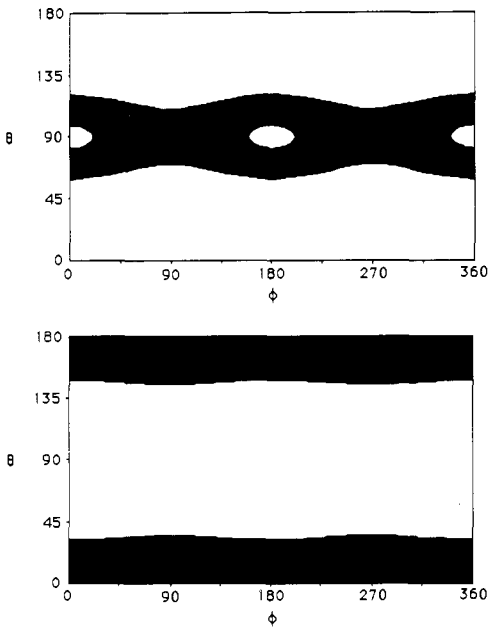

A (top), B (bottom)

Figure 6. θ/ϕ plots for the oriented ^{31}P CP NMR spectra with layer normal (A) perpendicular and (B) parallel to $\mathbf{B}_0$. The shaded regions indicate θ/ϕ combinations that are consistent with the experimental data.

only angles from 0 to 90° need be considered, since angles greater than 90° are related by symmetry. The range of chemical shifts exhibited in the perpendicular difference spectrum (Figure 5A) is −16 ± 10 ppm, corresponding to the θ/ϕ combinations shown in Figure 6A. From this plot, θ was limited to 59–90°. It is important to note that the θ/ϕ plots derived from the two difference spectra cannot be directly superimposed (after a 90° phase shift in θ) to further limit ϕ, since the uniaxial orientation does not allow correlation of ϕ from one plot to the other.

Each of these difference spectra independently suggests that the P–C bond is perpendicular to the $Zr(O_3P-)_2$ layers. This conclusion was arrived at by considering the orientation of σ_{33} in the molecular frame. Prior determination of the ^{31}P phosphonate chemical shielding tensor in $Zr(O_3PCH_2COOH)_2$ showed that σ_{33} lies 17° off the P–C bond.[8] The effect of ideal uniaxial orientation would therefore sweep out a $\theta = 17°$ cone when the layer normal is positioned parallel to $\mathbf{B}_0$ if the P–C bond was perpendicular to the $Zr(O_3P-)_2$ layers. With the layer normal perpendicular to $\mathbf{B}_0$, a 17° cone about $\theta = 90°$ would be swept out, resulting in a range of θ from 73 to 107°. Disorder in the molecular orientation on the glass slides was evaluated from the line widths of the oriented chemical shift frequency. The θ/ϕ plots include an additional range of θ of ca. 15° added to each 17° cone. Figure 7 shows simulated oriented spectra for the perpendicular (A) and parallel (B) layer normal orientations assuming that the P–C bond is perpendicular to the $Zr(O_3P-)_2$ layers and that the microcrystalline platelets are disorder by ±15° with respect to the glass slides.

Phosphorus-31 Spectra of $Zr(O_3P^{13}CH_2{}^{13}COOH)_2$. From analysis of the $^{31}P-^{13}C(H_2)$ dipolar perturbation of the ^{31}P powder pattern of $Zr(O_3P^{13}CH_2COOH)_2$, it was determined that $\beta = 17°$ and $D_{PC} = 2100$ Hz ($r_{PC} = 1.80$ Å).[8] The ^{31}P spectra of oriented, doubly labeled $Zr(O_3P^{13}CH_2{}^{13}COOH)_2$ allow independent confirmation of these values (and of the degree of sample disorder), since the line shapes exhibited in the spectra must be consistent with eqs 3 and 4 simultaneously. That is, one value of θ dictates both the observed chemical shift and the observed dipolar splitting for $\beta = 17°$ and $D_{PC} = 2100$ Hz. This is exactly what is observed in the $^{31}P-^{13}C$ dipolar coupled ^{31}P difference spectra obtained when the layer normal was placed perpendicular (Figure 8B) and parallel (Figure 8F) to $\mathbf{B}_0$. When the layer normal is perpendicular to $\mathbf{B}_0$, the angle between $\mathbf{B}_0$ and $\nu_{//PC}$ equals 90 ± 15° (vide supra),

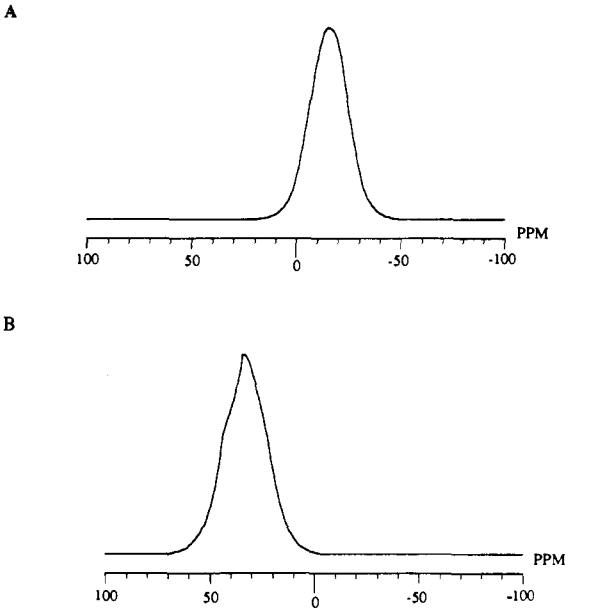

Figure 7. Simulated ^{31}P NMR spectra of oriented $Zr(O_3PCH_2{}^{13}COOH)_2$: (A) perpendicular and (B) parallel to $\mathbf{B}_0$ assuming a P–C bond perpendicular to the $Zr(O_3P-)_2$ layers and ±15° sample disorder.

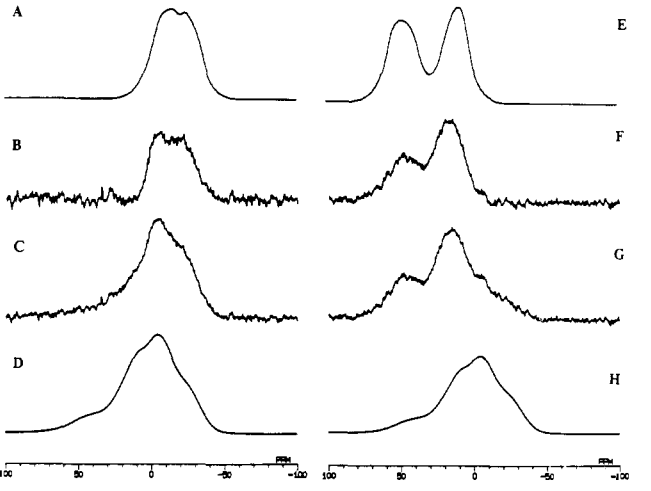

Figure 8. $^{31}P-^{13}C$ dipolar coupled ^{31}P NMR spectra of oriented $Zr(O_3P^{13}CH_2{}^{13}COOH)_2$: (A) perpendicular simulated spectrum, (B) perpendicular difference spectrum, (C) perpendicular experimental spectrum, (D) experimental powder spectrum, (E) parallel simulated spectrum, (F) parallel difference spectrum, (G) parallel experimental spectrum, and (H) experimental powder spectrum.

resulting in observed dipolar splitting ranging from 1680 Hz (at 75 and 105°) to 2100 Hz (at 90°). This additional range of splitting was observed superimposed on the perpendicularly-oriented ^{31}P spectrum of $Zr(O_3PCH_2{}^{13}COOH)_2$ (e.g., compare Figure 8B to 5A). When the layer normal is parallel to $\mathbf{B}_0$, the angle between $\mathbf{B}_0$ and $\nu_{//PC}$ equals 0 ± 15° (vide supra), and the observed dipolar splitting ranged from 3780 Hz (at ±15°) to 4200 Hz (at 0°). This additional range of splitting was observed superimposed on the parallelly-oriented ^{31}P spectrum of $Zr(O_3PCH_2{}^{13}COOH)_2$ (e.g., compare Figure 8F to 5D). Simulated spectra calculated from these ranges of $\mathbf{B}_0 - \nu_{//PC}$ angles and dipolar splittings are shown in Figure 8A,E for the perpendicular and parallel cases, respectively.

Carbon-13 NMR Spectra of $Zr(O_3PCH_2{}^{13}COOH)$. Oriented ^{13}C CP NMR spectra of ^{13}C-labeled $Zr(O_3PCH_2{}^{13}COOH)_2$ are shown in Figure 9. The left side of Figure 9 contains the experimental CSA powder pattern (C), the experimental spectrum with the layer normal perpendicular to $\mathbf{B}_0$ (B), and the difference spectrum (A), while the right side shows the analogous spectra

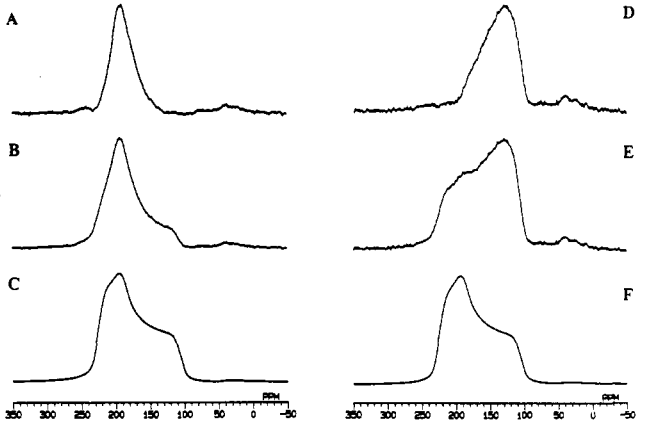

Figure 9. 67.9-MHz ^{13}C NMR spectra of oriented Zr-$(O_3PCH_2{}^{13}COOH)_2$: (A) perpendicular difference spectrum, (B) perpendicular experimental spectrum, (C) experimental powder spectrum, (D) parallel difference spectrum, (E) parallel experimental spectrum, and (F) experimental powder spectrum.

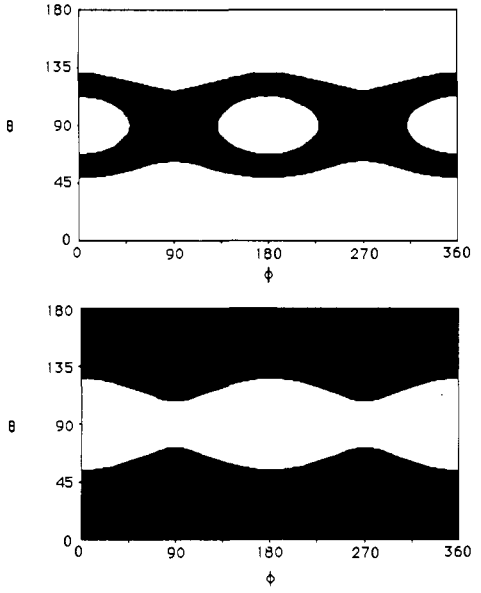

A (top), B (bottom)

Figure 10. θ/ϕ plots for the oriented ^{13}C CP NMR spectra with layer normal (A) perpendicular and (B) parallel to $\mathbf{B}_0$. The shaded regions indicate θ/ϕ combinations that are consistent with the experimental data.

obtained with the layer normal parallel to $\mathbf{B}_0$. Chemical shift frequency ranges of the difference spectra and the corresponding θ/ϕ plots were calculated as described above for the ^{31}P spectra using the chemical shielding principal elements extracted from the powder pattern of $Zr(O_3PCH_2{}^{13}COOH)_2$, i.e., $\sigma_{11} = -220$ ppm, $\sigma_{22} = -194$ ppm, and $\sigma_{33} = -108$ ppm. Chemical shifts range from 207 to 173 ppm in the perpendicular difference spectrum and 184 to 108 ppm in the parallel difference spectrum. θ/ϕ combinations consistent with these chemical shift ranges are shown in Figure 10, A and 1**B**, respectively. In the perpendicular case, θ was found to range from 50 to 90°; whereas in the parallel case, θ ranged from 0 to 70°.

Despite the large ranges for θ, certain conclusions could be drawn concerning the COOH plane orientation relative to the $Zr(O_3P-)_2$ layers when interpretation of the ^{13}C spectra was combined with results from analysis of the ^{31}P spectra and knowledge of the ^{13}C carboxyl chemical shielding tensor in the molecular frame. For this analysis, it was assumed that the P–C bond was perpendicular to the $Zr(O_3P-)_2$ layers and that the microcrystalline platelets of $Zr(O_3PCH_2{}^{13}COOH)_2$ were disordered ±15° relative to the glass slides. The orientation of the COOH plane relative to the $Zr(O_3P-)_2$ layers was defined in terms of the P–C–C–O dihedral angle, referred to here as ρ.

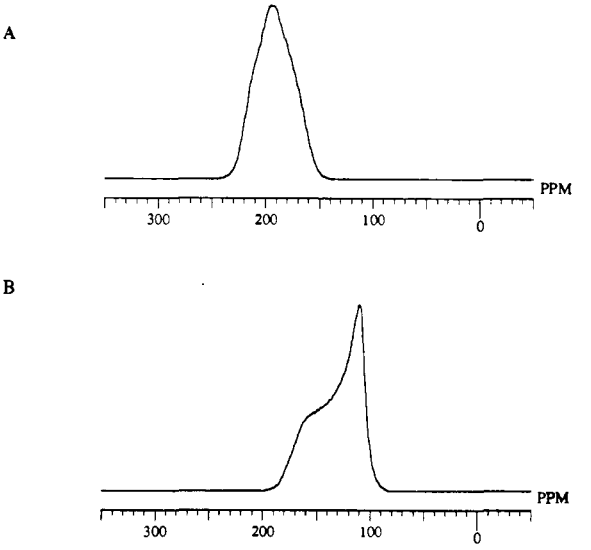

Figure 11. Simulated ^{13}C NMR spectra of oriented Zr-$(O_3PCH_2{}^{13}COOH)_2$: (A) perpendicular and (B) parallel to $\mathbf{B}_0$ assuming ρ = 75–90° and ±15° sample disorder.

To determine the range of values for ρ, the following method was used. First, the ±15° disorder was subtracted from the θ ranges determined from the ^{13}C perpendicular and parallel difference spectra to obtain the ranges expected for an ideally ordered sample. This subtraction resulted in new ranges of θ_{perp} = 65–90° for the perpendicular case and θ_{para} = 0–55° for the parallel case.[18] In this idealized situation, the minimum value of θ_{perp} corresponds to 90° minus the maximum possible value of θ_{para}. Thus, the maximum allowable value for θ_{para} is 25° for this sampling of "ideally" oriented platelets. From previous analyses, the P–C–C bond angle was determined to be ca. 110°,[8] which restricts θ in this idealized system to 20–90°, giving a minimum θ_{para} of 20°. Through geometric considerations (see Appendix) it can be established that for the ideally ordered crystallites

$$\cos \theta_{perp}/\cos \theta_{para} = \tan 20° \quad (6)$$

and

$$\rho = \sin^{-1} \sqrt{\cos^2 (\theta_{para})(1 + \tan^2 20°)} \quad (7)$$

therefore

$$\rho = \sin^{-1} \sqrt{\cos^2 (\theta_{perp})(1 + \tan^2 70°)} \quad (8)$$

From eq 7, ρ can be calculated to range from 75° (when θ_{para} = 25°) to 90° (when θ_{para} = 20°). Calculated perpendicular and parallel ^{13}C NMR spectra that reflect this range of ρ and the ±15° orientational disorder are shown in Figure 11. The range of dihedral angles, as shown in Figure 12, may be a reflection of the microcrystalline nature of zirconium phosphonates.

Conclusion

Analysis of solid-state ^{31}P and ^{13}C NMR difference spectra from uniaxially oriented films of $Zr(O_3PCH_2{}^{13}COOH)_2$ has allowed

(18) The range of θ_{para} is artificially large due to the method of calculation. As mentioned in the text, θ/ϕ plots were calculated from chemical shift frequency ranges that were taken as the full width at half maximum intensity. In calculation of θ/ϕ plots, only eq 3 was used; eq 4 was not incorporated. This method results in an artificially large θ range when there is a significant dipolar perturbation of the oriented spectrum. Since the unique element of the direct dipolar tensor for the $^{31}P-{}^{13}C(O)$ interaction lies ca. 30° from the $Zr(O_3P-)_2$ layer normal, the observed dipolar splitting in the parallel oriented spectrum is significantly larger than that observed in the perpendicularly-oriented spectrum. The same situation exists for the ^{31}P oriented spectra, as evidenced by Figure 5, A and D. An analogous situation also exists for the perpendicularly- and parallelly-oriented ^{31}P spectra of $Zr(O_3P{}^{13}CH_2{}^{13}COOH)_2$, Figure 8A,E, where the unique element of the direct dipolar tensor for the $^{31}P-{}^{13}C(H_2)$ interaction is coincident the $Zr(O_3P-)_2$ layer normal. For this reason, the more accurate θ_{perp} is used to limit θ_{perp}. The simulated spectra were calculated from both eqs 3 and 4.

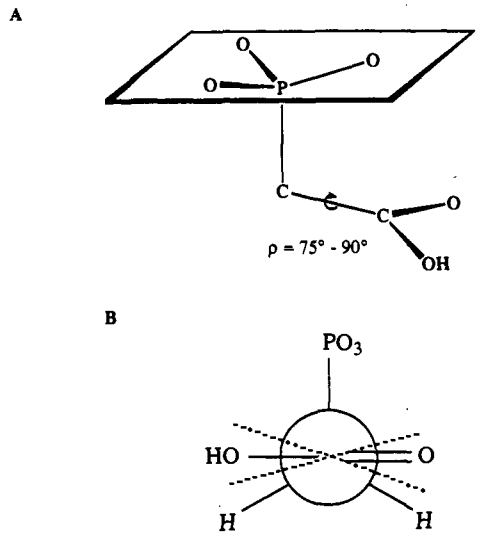

Figure 12. (A) Orientations of the P–C bond and COOH plane relative to the inorganic layers that are consistent with the experimental data. (B) Newman projection of a 90° P—C—C=O dihedral angle (ρ).

determination of the P–C bond and COOH plane orientations relative to the inorganic layers. The P–C bond was found to lie perpendicular to the inorganic $Zr(O_3–P–)_2$ layers, while the P–C–C–O dihedral angle was calculated as ranging from 75 to 90°. This is the first structural determination of a layered metal phosphonate by solid-state NMR. Investigations are now underway to elucidate structures of the organic pendant groups in other members of the $Zr(O_3P(CH_2)_nCOOH)_2$ family.

Experimental Section

All chemicals were purchased from Aldrich Chemical Company and were used as received. $Zr(O_3PCH_2{}^{13}COOH)_2$ was prepared according to the method of Dines and DiGiacomo[6] from $ZrOCl_2 \cdot 8H_2O$ and ^{13}C-labeled $(C_2H_5O)_2P(O)CH_2{}^{13}COOC_2H_5$. Powder XRD analysis (Philips Electronics Instruments; Cu Kα radiation) of $Zr(O_3PCH_2{}^{13}COOH)_2$ confirmed the reported interlayer spacing of 11.0 Å. The FT-IR spectrum (Nicolet 730 FT-IR spectrometer) of $Zr(O_3PCH_2{}^{13}COOH)_2$ exhibited a strong ^{13}C=O stretch at 1652 cm^{-1}, which is consistent with a ^{13}C isotope shift of the 1693 cm^{-1} C=O stretching absorption exhibited by nonlabeled $Zr(O_3PCH_2COOH)_2$.

Uniaxially oriented films of $Zr(O_3PCH_2{}^{13}COOH)_2$ were prepared by first sonicating a slurry of 0.1 g of $Zr(O_3PCH_2{}^{13}COOH)_2$ in 10 mL of ethanol for 1 h (1-s pulse, 50% duty cycle) in a cup-horn type sonicator (Heat Systems-Ultrasonics, Inc., Model W-385). Approximately 0.2 mL of the resulting dispersion was dropped onto each 6 × 22 mm piece of microscope slide cover glass and air dried. Twenty-five glass slips were stacked in a 7 mm o.d. sample cyclinder (one end left uncapped), which was then placed in the NMR probe coil at a 90° angle relative to $\mathbf{B}_0$. NMR spectra were obtained with the sample layer normal positioned parallel to $\mathbf{B}_0$ (i.e., slides lying one on top of another) and perpendicular to $\mathbf{B}_0$ (i.e., slides lying side by side).

Room temperature ^{13}C and ^{31}P solid-state NMR spectra were recorded at 67.9 and 109.4 MHz, respectively, on a JEOL 270 MHz spectrometer ($\mathbf{B}_0$ = 6.3 T) equipped with a 7-mm variable-angle sample spinning probe from Doty Scientific. High-power ^1H decoupling and cross polarization were employed for all spectra; a 50-kHz field strength was used for both ^1H decoupling and cross polarization. ^{13}C and ^{31}P signals were externally referenced to $Si(CH_3)_4$, and 85 wt % H_3PO_4, respectively (downfield shielding negative).

Simulated oriented chemical shift powder spectra, simulated oriented dipolar-coupled powder spectra, and θ/ϕ plots were calculated with programs written in this laboratory for use on a Macintosh computer. θ/ϕ plots were calculated from eq 3 by plotting θ/ϕ combinations that resulted in a chemical shift within the experimentally observed range of chemical shifts. The principal elements of the ^{31}P phosphonate and ^{13}C carboxyl chemical shielding tensors extracted from the CSA powder patterns of $Zr(O_3PCH_2COOH)_2$[8] were used in conjunction with eqs 1–5 to simulate spectra. Simulated spectra were calculated by integrating θ over 0 to π and ϕ over 0 to 2π in 1° increments. A sin θ intensity factor was used to approximate random sampling of all possible magnetic field vector orientations relative to the chemical shielding PAS. A Gaussian distribution function was used to simulate the ±15° disorder in the oriented spectra.

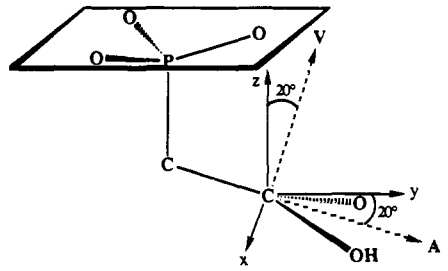

Figure 13. Description of the Cartesian coordinate system used in the derivation of eqs 6–8.

Acknowledgment. The purchase of the JEOL 270 NMR spectrometer was made possible by NSF Grant CHE-89-09857. Acknowledgment is also made to the donors of the Petroleum Research Foundation, administered by the American Chemical Society, and to the Air Force Office of Scientific Research (AFOSR-90-0122) for the support of this project.

Appendix. Derivation of Equations 6–8

A right-handed Cartesian coordinate system is defined with the origin at the carboxyl carbon, the z axis parallel with the P–C bond, and the y axis in the P–C–C plane. The unit vector, **A**, is defined as the extension of the C–C bond as shown in Figure 13. A second unit vector, **V**, is defined as coincident with the σ_{33} principal axis, which was determined to be perpendicular to **A**.[8] Rotation of **V** about **A** from the y–z plane toward the x-axis is defined in terms of the P–C–C–O dihedral angle, ρ, such that ρ = 90° when **V** is in the y–z plane and ρ = 0° when **V** is along the x axis. Since vector **A** is orthogonal to vector **V** and will remain orthogonal throughout the rotation, the vector product can be written

$$(V_x,V_y,V_z)(A_x,A_y,A_z) = 0 \qquad \text{(A-1)}$$

When ρ = 90°, the components of **A** in the x, y, and z directions are $A_x = 0$, $A_y = \cos 20°$, and $A_z = -\sin 20°$, respectively, so that eq A-1 can be evaluated as

$$(V_x,V_y,V_z)(0,\cos 20°,-\sin 20°) = 0 \qquad \text{(A-2)}$$

$$V_x(0) + V_y \cos 20° - V_z \sin 20° = 0 \qquad \text{(A-3)}$$

$$V_y = V_z \tan 20° \qquad \text{(A-4)}$$

The rotation of the unit vector **V** about **A** sweeps out a circle on the surface of a sphere, so that for any ρ, the point on the circle can be described by the following equation

$$V_x^2 + V_y^2 + V_z^2 = 1 \qquad \text{(A-5)}$$

Substituting for V_y according to eq A-4 gives

$$V_x^2 + (V_z \tan 20°)^2 + V_z^2 = 1 \qquad \text{(A-6)}$$

therefore

$$V_x^2 + V_z^2(1 + \tan^2 20°) = 1 \qquad \text{(A-7)}$$

The value of V_x can be described by

$$V_x = \cos \rho \qquad \text{(A-8)}$$

Substituting this relationship for V_x into eq A-7 gives

$$\cos^2 \rho + V_z^2(1 + \tan^2 20°) = 1 \qquad \text{(A-9)}$$

and solving for V_z

$$V_z = \sqrt{\frac{1 - \cos^2 \rho}{1 + \tan^2 20°}} \qquad \text{(A-10)}$$

Now, V_z can be defined in terms of θ when the layer normal is parallel to B_0 as

$$V_z = \cos \theta_{para} \quad \text{(A-11)}$$

and substituting eq A-11 into eq A-10

$$\theta_{para} = \cos^{-1} \sqrt{\frac{1 - \cos^2 \rho}{1 + \tan^2 20°}} \quad \text{(A-12)}$$

rewriting eq A-12 using the relationship $\sin^2 \rho + \cos^2 \rho = 1$

$$\theta_{para} = \cos^{-1} \sqrt{\frac{\sin^2 \rho}{1 + \tan^2 20°}} \quad \text{(A-13)}$$

or, in terms of θ_{perp},

$$\theta_{perp} = \cos^{-1} \sqrt{\frac{\sin^2 \rho}{1 + \tan^2 70°}} \quad \text{(A-14)}$$

Equation A-13 can be rewritten as

$$\cos^2 \theta_{para} = \frac{\sin^2 \rho}{1 + \tan^2 20°} \quad \text{(A-15)}$$

or

$$\rho = \sin^{-1} \sqrt{\cos^2 (\theta_{para})(1 + \tan^2 20°)} \quad \text{(A-16)}$$

and eq A-14 can be rewritten as

$$\cos^2 \theta_{perp} = \frac{\sin^2 \rho}{1 + \tan^2 70°} \quad \text{(A-17)}$$

or

$$\rho = \sin^{-1} \sqrt{\cos^2 (\theta_{perp})(1 + \tan^2 70°)} \quad \text{(A-18)}$$

and therefore

$$\cos \theta_{perp} / \cos \theta_{para} = \tan 20° \quad \text{(A-19)}$$

Well-Defined Redox-Active Polymers and Block Copolymers Prepared by Living Ring-Opening Metathesis Polymerization

D. Albagli, G. Bazan, M. S. Wrighton,* and R. R. Schrock*

Contribution from the Department of Chemistry, Massachusetts Institute of Technology, Cambridge, Massachusetts 02139. *Received June 13, 1991. Revised Manuscript Received January 30, 1992*

Abstract: Mo(CH-*t*-Bu)(NAr)(O-*t*-Bu)$_2$ (**1a**) in THf/0.1 M [*n*-Bu$_4$N]AsF$_6$ is not oxidized at potentials up to 1.0 V and undergoes a reversible, one electron reduction at −2.16 V vs SCE at a Pt electrode. An analogous intiator containing a ferrocenylmethylidene ligand (**1b**) can be synthesized by treating **1a** with vinylferrocene. Redox-active derivatives of norbornene, containing ferrocene (**2**) or phenothiazine (**3**), were prepared and polymerized by **1a** or **1b** to give living block copolymers containing the ring-opened norbornene derivatives. The living polymer was cleaved from the metal in a Wittig-like reaction with pivaldehyde, trimethylsilylbenzaldehyde, or octamethylferrocenecarboxaldehyde. Polydispersities for the longer block copolymers containing up to ~80 monomer units were found to be as low as 1.05 by GPC. In one case the polydispersity of a homopolymer made from the ferrocene-containing monomer was determined by FD-mass spectroscopy to be 1.06. DSC studies suggest that microphase formation occurs in the block copolymers, even in the case of relatively low molecular weight materials. Solution voltammetric studies of homo and block copolymers showed that the redox centers were electrochemically independent and that all centers exchanged electrons with the electrode. Neutral polymers became insoluble upon oxidation to a polycation, yielding an adsorbed polymer layer on the electrode that could then be cathodically stripped. This oxidative deposition process depended on the electrolyte and the polymer molecular weight but also could be controlled by the size of a nonelectroactive block in the block copolymers. Problems resulting from precipitation of the redox polymers could be circumvented by employing normal pulse voltammetry. Polymers containing redox centers in both end groups as well as in the polymer chain itself have been prepared and their nature confirmed in electrochemical studies.

Introduction

Studies of electroactive polymers attached to the surface of electrodes have focused primarily on electrochemical characteristics, and modification of electrodes with such polymers in order to achieve "molecular electronic" functions, such as pH-dependent charge trapping and chemical sensing,[1] has been successful to some degree. Ideally, however, one would like to be able to control the primary structure and the morphology of a polymer attached to an electrode to a degree that would maximize the desired electrochemical properties. The primary structure of an electroactive polymer, and ultimately its morphology (lamellae, rods, or spheres), could be controlled if living polymerization techniques could be employed.[2] Under such circumstances (no chain transfer or termination) the nature of the functionality at each end of the polymer as well as the nature and length of blocks (containing a given monomer) in the polymer chain could be specified. However, traditional living anionic polymerization methods[3] probably cannot be employed routinely, since relatively sensitive, redox-active groups would be destroyed. Cationic[4] or group transfer methods[5] might be more suitable than anionic methods but again some desirable functionalities may not be tolerated. Living ring opening metathesis polymerization (ROMP) of nor-

(1) (a) Smith, D. K.; Tender, L. M.; Lane, G. A.; Licht, S.; Wrighton, M. S. *J. Am. Chem. Soc.* **1989**, *111*, 1099. (b) Shu, C.-F.; Wrighton, M. S. *J. Phys. Chem.* **1988**, *92*, 5221.

(2) (a) Odian, G. *Principles of Polymerization*; Wiley: New York, NY, 1981. (b) Rempp, P.; Merrill, E. *Polymer Synthesis*; Huethig & Wepf: Heidelberg, 1986. (c) Gold, L. *J. Chem. Phys.* **1958**, *28*, 91. (d) Flory, P. *J. Am. Chem. Soc.* **1940**, *62*, 1561. (e) Szwarc, M. *Nature* **1956**, *178*, 1168.

(3) Szwarc, M. *Carbanions, Living Polymers, and Electron Transfer Processes*; Wiley: New York, 1968.

(4) Miyamoto, M.; Sawamoto, M.; Higashimura, T. *Macromolecules* **1984**, *17*, 265.

(5) Sogah, D. Y.; Webster, O. W. *Macromolecules* **1986**, *19*, 1775.

0002-7863/92/1514-4150$03.00/0 © 1992 American Chemical Society